NeuroImage 257 (2022) 119309

Contents lists available at ScienceDirect

NeuroImage

journal homepage: www.elsevier.com/locate/neuroimage

Neuroanatomical foundations of delayed reward discounting decision making II: Evaluation of sulcal morphology and fractal dimensionality

Carly McIntyre-Wood[a], Christopher Madan[b], Max Owens[a], Michael Amlung[c,e], Lawrence H. Sweet[d], James MacKillop[a,*]

[a] Peter Boris Centre for Addictions Research, McMaster University & St. Joseph's Healthcare Hamilton, Hamilton, ON, Canada
[b] School of Psychology, University of Nottingham, Nottingham, United Kingdom
[c] Cofrin Logan Center for Addiction Research and Treatment, Lawrence, KS, United States of America
[d] Department of Psychology, University of Georgia, Athens, GA, United States of America
[e] Department of Applied Behavioural Sciences, University of Kansas, Lawrence, KS, United States of America

ARTICLE INFO

Keywords:
Delayed reward discounting
Sulcal morphology
Fractal dimensionality
MRI
Behavioral economics

ABSTRACT

Delayed reward discounting (DRD) is a form of decision-making reflecting valuation of smaller immediate rewards versus larger delayed rewards, and high DRD has been linked to several health behaviors, including substance use disorders, attention-deficit/hyperactivity disorder, and obesity. Elucidating the underlying neuroanatomical factors may offer important insights into the etiology of these conditions. We used structural MRI scans of 1038 Human Connectome Project participants (M_{age} = 28.86, 54.7% female) to explore two novel measures of neuroanatomy related to DRD: 1) sulcal morphology (SM; depth and width) and 2) fractal dimensionality (FD), or cortical morphometric complexity, of parcellated cortical and subcortical regions. To ascertain unique contributions to DRD preferences, indicators that displayed significant partial correlations with DRD after family-wise error correction were entered into iterative mixed-effect models guided by the association magnitude. When considering only SM indicators, the depth of the right inferior and width of the left central sulci were uniquely associated with DRD preferences. When considering only FD indicators, the FD of the left middle temporal gyrus, right lateral orbitofrontal cortex, and left lateral occipital and entorhinal cortices uniquely contributed DRD. When considering SM and FD indicators simultaneously, the right inferior frontal sulcus depth and left central sulcus width; and the FD of the left middle temporal gyrus, lateral occipital cortex and entorhinal cortex were uniquely associated with DRD. These results implicate SM and FD as features of the brain that underlie variation in the DRD decision-making phenotype and as promising candidates for understanding DRD as a biobehavioral disease process.

1. Introduction

An individual's propensity to value smaller more immediate rewards over larger delayed rewards is referred to as delayed reward discounting (DRD). While all individuals devalue future rewards to a certain extent, heightened levels of DRD are of interest to various health behaviors, including psychoactive substance use (MacKillop et al., 2011; Amlung et al., 2017), pathological gambling (Dixon et al., 2003; MacKillop et al., 2014), obesity (Amlung et al., 2016), attention-deficit/hyperactivity disorder (Rosch and Mostofsky, 2015; Wilson et al., 2011; J.N. Jackson and MacKillop, 2016), bipolar disorder (Urošević et al., 2016), and schizophrenia (Horan et al., 2017). Moreover, given its implication underlying these disorders, DRD has been proposed to be a trans-disease mechanism (Bickel et al., 2012). Consequently, elucidating the neuroanatomical foundations of elevated DRD may contribute to understanding risk for numerous health behaviors and guide brain-based treatment strategies (e.g., neuromodulation; Manuel et al., 2019; Cho et al., 2015).

A relatively small number of studies have examined the underlying structural substrates of DRD, primarily focusing on differences in gray matter volume (GMV), cortical thickness (CT), and surface area. More specifically, research in healthy participants has revealed significant associations between elevated discounting of rewards and reductions in cortical structure indicators, including decreased GMV of the inferolateral prefrontal cortex (PFC), decreased GMV, CT and cortical surface area of the dorsolateral PFC (Bjork et al., 2009; Drobetz et al., 2014) and decreased GMV of the orbitofrontal cortex (OFC; Li et al., 2019). Regarding subcortical structures, volume reductions of the bilateral ventral putamen and prefrontal subgyral area and increased volume

* Corresponding author.
E-mail address: jmackill@mcmaster.ca (J. MacKillop).

https://doi.org/10.1016/j.neuroimage.2022.119309.
Received 22 November 2021; Received in revised form 1 April 2022; Accepted 10 May 2022
Available online 19 May 2022.

of the parahippocampus have also been reported in relation to heightened DRD (Cho et al., 2013; Yu, 2012). Studies have also linked elevated DRD to greater indicators of cortical structure. Opposing the findings of Li et al. (2019), Cho et al. (2013) found that increased GMV and CT of the orbitofrontal gyrus was related to increased discounting of delayed rewards. Increased GMV in relation to elevated DRD in the bilateral anterior cingulate cortex (ACC; Li et al., 2019), medial frontal gyri, left middle cingulate (Cho et al., 2013), left middle frontal gyri, and the right frontal pole (FP; Wang et al., 2016) have also been reported. Apart from GMV, increased CT of the left lateral FP and increased cortical surface area of the left FP and OFC, and mid ACC have also been linked to elevated DRD (Drobetz et al., 2014). These contrasting reports of cortical alterations related to increased DRD may reflect differential localized patterns of cortical structure underlying aberrant DRD; however, due to predominantly small sample sizes, discrepant sample ages (e.g., adolescents, seniors), varying scanner resolution (i.e., 1.5 Tesla or 3.0 Tesla) and DRD task format, and consideration of only specific regions of interest (ROIs) rather than the whole brain, the comparability and external validity of these structural findings may be limited. To address limitations in structural DRD research, Owens et al. (2017) completed a study systematically examining the neuroanatomical correlates of DRD using GMV of parcellated cortical and segmented subcortical regions of the brain in a large sample (n = 1038) from the Human Connectome Project (HCP). Results of the study indicated that lower total cortical GMV of the bilateral middle temporal gyrus (MTG) and entorhinal cortex (EC) were unique and significant predictors of DRD, accounting for 7.7% of the variance. Subcortical regions did not display any significant relations with DRD .

To delineate the neuroanatomical substrates of DRD, there may be utility in comparing findings from structural MRI to those from functional MRI and non-invasive brain stimulation (e.g., repetitive transcranial stimulation [rTMS]). However, research has indicated that alterations in functional activity do not necessarily correspond to structural differences (Owens et al., 2018). More prosaically, just because an area displays aberrant activity or connectivity during a DRD task, it may not display any difference in structure (e.g., volume, thickness, FD). Research using functional imaging techniques have identified several regions of interest (ROIs) to DRD decision-making, including regions of the frontal pole (i.e., ventromedial PFC and lateral frontopolar cortex; Wang et al., 2016), other regions of the PFC (ie., left dorsolateral PFC and medial PFC; Kable and Glimcher, 2007; Cho et al., 2015), middle temporal and frontal gyri (MacKillop et al., 2012), and the insular and anterior cingulate cortices (MacKillop et al., 2012; Yang et al., 2022. However, while various theories exist, research is not unanimous on the roles of these ROIs (McClure et al., 2004; Kable and Glimcher, 2007). The importance of the FP to DRD decision-making has been substantiated by Wang et al. (2016) who used resting-state functional connectivity (rsFC) to demonstrate that increased discounting of delayed rewards was associated with lowered connectivity between the FP and the ventromedial PFC. Multiple task-based functional MRI studies have also supported roles of the ventral striatum, ventromedial PFC, and PCC in internal calculations of the subjective value of delayed rewards (Kable and Glimcher, 2007; Peters and Buchel, 2009; Chib et al., 2009). While the ventral striatum, ventromedial PFC, and PCC are believed to establish subjective value based on more emotional factors, the left dorsolateral PFC appears to integrate more "rational" cognitively relevant information to decision-making (McClure et al., 2004). This is believed to occur through a modulatory role on subjective value perceptions established in the ventromedial PFC, as demonstrated by Hare and colleagues (2014) who found that the dorsolateral PFC is most active when participants select larger delayed rewards. Further, Hare et al. (2014) found that connectivity between the dorsolateral and ventromedial PFC was increased during DRD decisions, especially those where delayed rewards were selected. The importance of regions within the PFC has also been supported by rTMS studies which have found that modulating medial PFC excitability using high-frequency rTMS reduced discounting of future rewards compared to rTMS on a control site (Cho et al., 2015) and that disruption of the left lateral PFC using low-frequency rTMS increased preferences for immediate rewards (Figner et al., 2010). Sulcal morphology (SM) and fractal dimensionality (FD) are two novel measures of brain morphometry that have the potential to aid in the elucidation of the neuroanatomical underpinnings of DRD. The first, sulcal morphology, assesses the morphology of the cortex by estimating the width and depth of several major sulci of the brain. Traditionally, cortical morphology has been assessed using measurements of GMV, cortical thickness, surface area, or gyrification (Madan, 2019). Enlargement of cortical sulci has been established as a natural representation of age-related atrophy (Drayer, 1988), however, research has demonstrated that the degree of atrophy varies greatly between individuals and regions of the brain (Coffey, 1992). The utility of SM as a diagnostic criterion for Alzheimer's disease (AD) has also recently been demonstrated in a study by Bertoux et al. (2019), wherein they found that sulcal width was a better predictor of AD than sulcal cortical thickness, regional cortical volume, cortical thickness, and hippocampal volume. Similar results have also been found in other studies investigating the same relationship (Hamelin et al., 2015). Furthermore, as SM analysis is not dependent on gray and white matter contrast, it is a more resilient measure to study pathological processes in which the contrasts weaken (Bertoux, 2019).

Fractal dimensionality, originally conceived as fractional dimensionality, is a measure of the geometric complexity of irregular natural structures (e.g., coastlines, clouds, snowflakes) that cannot be assessed in standard parameters like the solid figures of conventional or Euclidian geometry (e.g., circles). While the original mathematical theories were largely developed in the late 19th and early 20th centuries, the term FD was not popularized until 1975 when by Benoît Mandelbrot coined the term based on the Latin word *fractus* meaning "fragmented" or "broken" (Mandelbrot, 1985). Etymologically, Mandelbrot also related the term to the word fraction, meaning between integers, as the fractal set of an irregular structure lies between Euclid shapes (Mandelbrot, 1985). FD has since been applied to complex biological components of the human body, including liver histopathological structures, microvasculature of histological specimens, and various aspects of the brain such as the cerebral cortex (Grizzi et al., 2001; Reishofer et al., 2018). Pertaining to the brain, alterations in FD have been linked to several conditions, including significant reductions in the cortical FD of mild Alzheimer's (King et al., 2010) and acute anorexia nervosa patients (Collantoni et al., 2020), and decreased white matter FD in multiple sclerosis patients (Esteban et al., 2009). FD has not yet been investigated in relation to DRD; however, as it has been shown to be more sensitive to age-related cortical and subcortical alterations than CT or gyrification index (Madan and Kensinger, 2016), FD may offer insights on structural substrates of DRD beyond traditional measures.

Given the small literature on the neuroanatomical underpinnings of DRD, the associated limitations (e.g., small sample sizes, subgroup focus, and low resolution), and the promise of these novel cortical measurements, the current study seeks to investigate SM and FD in relation to DRD. Specifically, the current study aims to extend the previous HCP findings by Owens et al. (2017) by examining: 1) the width and depth of eight major sulci of the brain and 2) parcellated cortical and segmented subcortical complexity as measured by FD using the Desikan atlas for neuroanatomical localization. Based on previous literature on the neural correlates of DRD, we expected to find that alterations in SM and FD in sulcal regions and cortical parcels within the PFC and frontal pole (in particular the dorsolateral, inferolateral, and ventromedial PFC (Bjork et al., 2009; Wang et al., 2016; Hare et al., 2014; Koechlin, 2011), the OFC (Drobetz et al., 2014), and the PCC (Kable and Glimcher, 2007; Peters and Buchel, 2009; Chib et al., 2009) would be associated with DRD decision-making. Further, we postulated reduced FD in the bilateral entorhinal cortex and middle temporal gyri as lowered GMV of these parcels was shown to be significantly associated with DRD by Owen and colleagues (2017) in the same dataset. Finally, given research has shown SM to be a better Alzheimer's predictor than CT

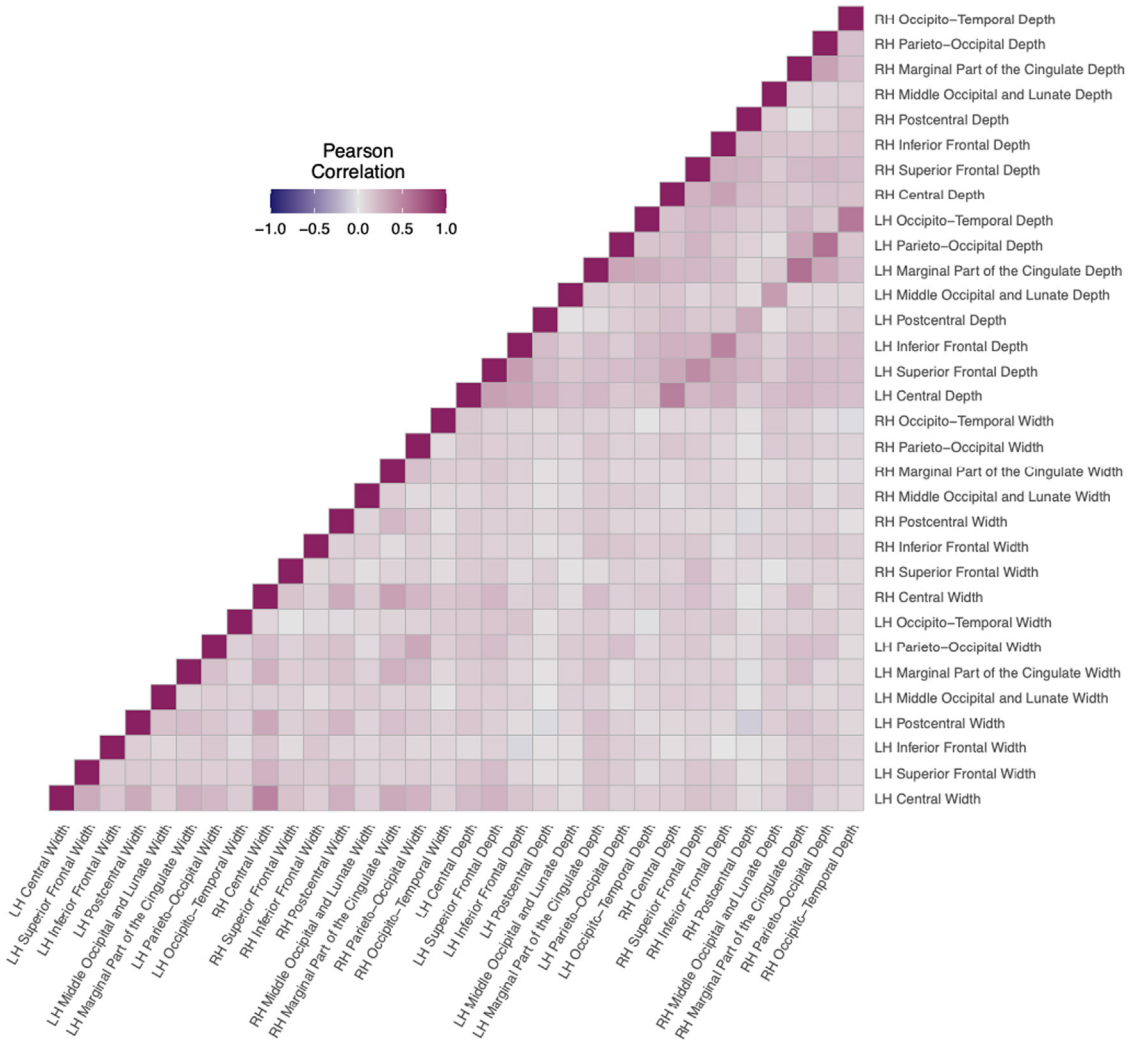

Fig. 1. Pearson correlation matrix represented as a heatmap for sulcal morphology regions. Sulcal Depth (Median = .194, IQR = .098); Sulcal Width (Median = .117, IQR = .077); Combined Sulcal Width and Depth (Median = .117, IQR = .088).

and volume (Bertoux et al., 2019) and that FD is more sensitive to age-related changes than volume (Madan, 2021), we postulated that SM and FD measures would account for more variance than using GMV alone.

2. Results

2.1. Sulcal morphology

The zero-order correlation matrix displaying all SM regions expressed as a heatmap is shown in Fig. 1. Correlations ranged from 0.13 between the widths of the left and right middle occipital and lunate and occipito-temporal sulci to 0.61 between the depths of the left and right marginal part of the cingulate sulcus, indicating that only 1.7–37.2% of variance was shared across homologous sulci. Given this finding, sulcal measures were examined separately by hemisphere.

When considering significant associations between SM and DRD, quantified using a mean area under the curve (mAUC) discounting measure, reduced sulcal width and depth were consistently associated with increased mAUC, or less steep DRD. Of the 16 sulcal depth measurements examined, greater depths of 7 sulci were significantly associated with greater mAUC. These included the depths of the left marginal part of the cingulate, right post-central, left inferior frontal, right central, left superior frontal, left central, and right inferior frontal sulci, in ascending order of correlation magnitude. Of the 16 sulcal width measurements, greater widths of 4 sulci displayed significant positive associations with mAUC: the right superior frontal, right central, and left central sulci, in ascending order of correlation magnitude. The depth of the right inferior frontal sulcus and the width of the left central sulcus maintained a significant association with mAUC after family-wise error (FWE) correction (see Supplemental Table 1).

Of the two SM measures that survived FWE correction, the depth of the right inferior frontal sulcus displayed the lowest FWE-corrected *p*-value and was added to the linear mixed-effects model first. The remaining significant SM measure, the width of the left central sulcus, was then added to the model to see if it offered unique significant variance. Both displayed significant unique effects on DRD, resulting in a final linear mixed-effects model including the right inferior frontal sulcal depth and left central sulcal width (see Fig. 2). Income was the only covariate that exhibited a significant effect in the model, with lower income being associated with decreased mAUC, or increased DRD. The final model is presented in Table 1 and accounted for 4.7% and 30.8% of marginal and conditional variability in mAUC, respectively.

2.2. fractal dimensionality

The zero-order correlation matrix for FD of cortical parcels expressed as a heatmap are displayed in Fig. 3. Correlations between the FD of cortical parcels in the right and left hemispheres ranged from .29 in cau-

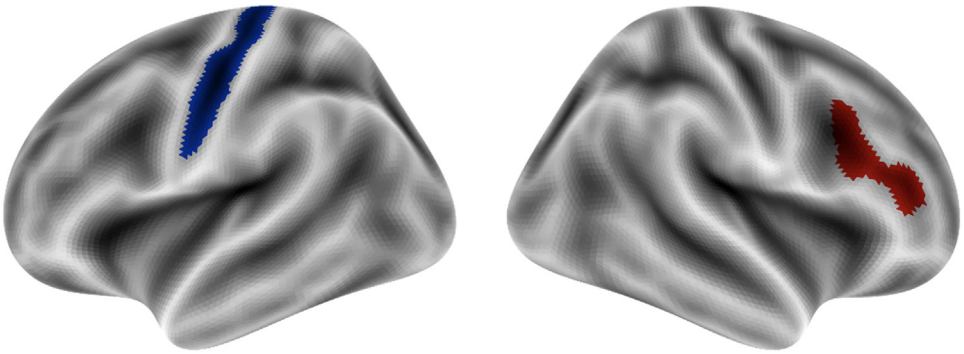

Fig. 2. Sulcal morphology regions that exhibited unique significant effects on area under the curve delay discounting measure. Blue = Left Central Sulcus Width, Red = Right Inferior Frontal Sulcus Depth.

Table 1
Final linear mixed-effects model including sulcal width and depth as predictors of an area under the curve discounting measure.

	F	*B*	*SE*	*t*	*P*	Δ Marginal R^2/ Combined Marginal R^2
Covariate Model						.025/.047
Sex	0.670	−0.015	0.019	−0.819	.413	–
Age	0.327	−0.001	0.002	−0.572	.567	–
Income	8.602	0.010	0.003	2.933	.003	–
Dizygotic Twin Status	0.029	0.003	0.020	0.170	.865	–
Monozygotic Twin Status	0.004	0.001	0.017	0.062	.951	–
Total Intracranial Volume	1.169	0.011	0.010	1.081	.280	–
Morphometry Indicators						.022/.047
R Inferior Frontal Sulcal Depth	14.127	0.015	0.004	3.759	1.8E-4	.014
L Central Sulcal Width	7.108	0.041	0.015	2.666	.008	.008

Note. *R*= Right. *L*= Left. SE = Standard Error. Only regions with significant *p*-values after family-wise error correction are included ($p_{FWE} < 0.05$) Delay discounting was assessed using mean area under the curve for $200 and $40,000 tasks. Smaller area under the curve is indicative of higher delayed reward discounting.

dal anterior cingulate cortex to .79 in the insula; indicating that 8.4% – 62.4% of variance was shared across homologous cortical regions. Given this finding, cortical FD measures were examined separately by hemisphere. Of the 62 cortical FD measures included in the study, FD of 10 parcels were significantly associated with mAUC after FWE correction. Regions in which cortical FD was significantly correlated with mAUC following FDR correction are listed in order of magnitude in Supplementary Table 2. In all cases, higher cortical FD was associated with higher mAUC, or less steep DRD. As Owens et al. (2017) did not find significant associations between subcortical GMV and to reduce type I error rate, the FD of subcortical structures were tested as bilaterally combined measures. No significant associations were observed. Correlations between the FD of subcortical measures are available in Supplementary Figure 1.

The results of the final mixed-effects model exploring parcellated cortical FD with mAUC as the dependant variable are visible in Table 2. The final model indicated that the FD of four parcellated cortical regions exhibited unique significant contributions to mAUC: the left middle temporal gyrus, right lateral OFC, left lateral occipital cortex, and left entorhinal cortex (See Fig. 4 for a visual representation). Among the covariates in the model, only sex and income exhibited significant effects, with female sex and lower income being associated with greater DRD. The final model accounted for 7.2% and 29.6% of marginal and conditional variability in mAUC, respectively.

2.3. Integrated analysis

Supplementary Table 3 displays SM and FD measures that displayed significant partial correlations with mAUC after FWE correction, ranked in order correlation magnitude. Taken together, there were 2 SM and 10 FD regions with significant FWE-corrected associations with mAUC. In all cases, greater FD or sulcal width and depth was associated with greater mAUC, or less steep DRD. The final linear mixed-effects model is visible in Table 4. Of the 12 regions included in the integrated iterative analysis, 5 measures produced significant independent effects on mAUC: FD of the left middle temporal gyrus and left lateral occipital and entorhinal cortices; depth of the right inferior frontal sulcus; and width of the left central sulcus. The final model accounted for 8.2% and 32.9% of marginal and conditional variability in mAUC, respectively. Among the covariates in the model, sex and income exhibited significant effects, with female sex and lower income being associated with greater DRD.

Table 3

When including GMV regions which were found to be significant predictors of mAUC by Owens et al. (2017), correlations surviving FWE correction are visible in Supplemental Table 4. In all cases, higher FD, larger sulcal width, and greater GMV were associated with higher mAUC, or less steep DRD. The final linear mixed-effects model is displayed in Table 4. Of the 15 FWE-corrected indicators included in the iterative linear mixed-effects model analysis, 4 displayed unique contributions to mAUC: FD of the left middle temporal gyrus, GMV of the left entorhinal cortex, FD of the left lateral occipital cortex, and the depth of the right inferior frontal sulcus. The final model accounted for 7.7% and 32.9% of marginal and conditional variability in mAUC, respectively. Among the covariates in the model, income exhibited significant effects, with lower income being associated with greater DRD.

3. Discussion

The current study sought to elucidate the neuroanatomical underpinnings of DRD by examining two novel measures: SM and FD. Analysis of SM revealed that of the 16 sulcal width and 16 sulcal depth measurements, 2 were significantly associated with DRD after FWE correction, and 2both predicted unique variance in DRD preferences: 1) the depth of the right inferior frontal sulcus, and 2) the width of the left central sulcus. In both cases, decreased depth and width were associated with increased discounting of future rewards. The finding of increased depth of the right inferior frontal sulcus supports our initial hypothesis that SM alterations associated with elevated DRD would be present

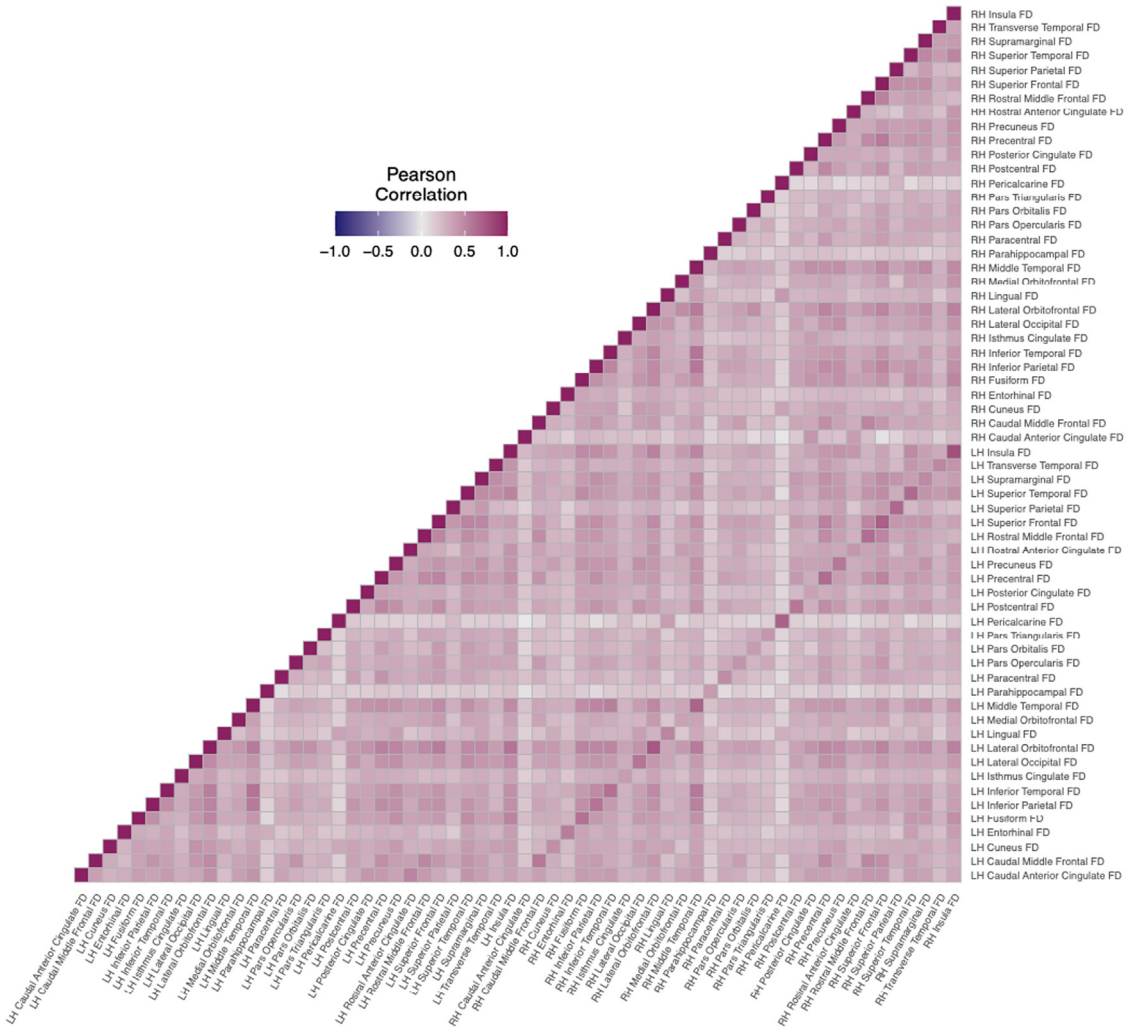

Fig. 3. Pearson correlation matrix represented as a heatmap for parcellated cortical fractal dimensionality (Median = .311, IQR = .140).

within the PFC, whereas the central sulcus finding does not. This hypothesis was based on previous structural findings that found reduced measures of cortical structure including (e.g., GMV, CT, and cortical surface area) within the dorsolateral PFC, inferolateral PFC, and OFC in relation to increased discounting of delayed rewards (Bjork et al., 2009; Drobetz et al., 2014; Li et al., 2019).

The depth of the right inferior frontal sulcus, which lies between the inferior and middle frontal gyri in the lateral PFC (Guenther et al., 2015), was negatively correlated with DRD and predicted the highest amount of unique variance in DRD behavior. The relevance of this finding is supported by previous research implicating the right inferior frontal gyrus as a key cortical region for inhibitory control (Aron et al., 2014; Cai et al., 2017). This finding relates to DRD as research suggests that cognitive control is necessary to select delayed over immediate rewards (McClure et al., 2004) . This finding also adds to a bulk of literature demonstrating the importance of regions in the lateral PFC to DRD behavior (Drobetz et al., 2014; Wang et al., 2016; Hare et al., 2014). As a whole, the inferior frontal sulcus also appears to have a key functional role in working memory (Demanet et al., 2016); a brain system used to store and manipulate temporary information that is pivotal for effective learning and reasoning (Baddeley, 1992). More specifically, the inferior frontal sulcus is believed to play a role in procedural WM, a subtype of WM used for applying instructions (Demanet et al., 2016). The link between DRD and WM has been substantiated in the literature and appears to be due to the need for executive WM to effectively consider two choices, their associated costs and benefits, and an individual's own short-term and long-term goals (Bickel et al., 2011; Finn et al., 2015). Taken together, it is conceivable that altered SM of the inferior frontal sulcus may be related to DRD through deficits in reward benefit formulations and retrieving those formulations during decision making (Bickel et al., 2007). The width of the left central sulcus, which divides the primary motor and somatosensory areas (Li et al., 2015), predicted the second-highest amount of unique variance in DRD among sulcal measures, with reduced width being associated with increased devaluation of future rewards. This finding was not expected, however, may be of interest as research has demonstrated a link between central sulcal morphology and ADHD (Li et al., 2015). Specifically, Li et al. (2015) found that central sulcus depth was significantly larger in children with ADHD compared to controls, while other measures, such as average span and surface area, were not. The authors attributed these structural changes in the motor cortex to ADHD symptomology (Li et al., 2015). Given that ADHD is associated with elevated DRD (Jackson and MacKillop, 2016), this finding warrants further exploration.

These results demonstrate regional heterogeneity in SM in relation to DRD preferences. While SM in the context of DRD preferences has not been previously explored, the central and inferior frontal (Madan, 2019; Jin et al., 2018) sulci appear to be particularly sensitive to age-related atrophy. However, while age-related atrophy is generally associated with more wide and shallow sulci, higher DRD in the current study was asso-

Table 2
Final hierarchical regression model including fractal dimensionality of cortical parcels as predictors of an area under the curve discounting measure.

	F	*B*	*SE*	*t*	*p*	Δ Marginal R^2/ Combined Marginal R^2
Covariate Model						.025/.072
Sex	2.782	−0.031	0.019	−1.708	.096	–
Age	0.243	0.001	0.002	0.632	.622	–
Income	9.818	0.011	0.003	3.095	.002	–
Dizygotic Twin Status	0.004	0.001	0.020	0.083	.952	–
Monozygotic Twin Status	0.221	−0.008	0.017	−0.434	.638	–
Total Intracranial Volume	0.475	−0.007	0.011	−0.689	.491	–
Morphometry Indicators						.047/.072
L Middle Temporal Gyrus FD	8.497	1.045	0.359	2.915	.004	.022
R Lateral OFC FD	4.205	0.903	0.440	2.051	.041	.011
L Lateral Occipital Cortex FD	6.939	0.945	0.359	2.634	.009	.008
L Entorhinal Cortex FD	7.092	0.494	0.185	2.663	.008	.006

Note. FD= Fractal Dimensionality. *L* = Left. *R* = Right. OFC = Orbitofrontal Cortex. SE = Standard Error. Only regions with significant *p*-values after family-wise error correction are included ($p_{FWE} < 0.05$). Delay discounting was assessed using mean area under the curve for $200 and $40,000 tasks. Smaller area under the curve is indicative of higher delayed reward discounting.

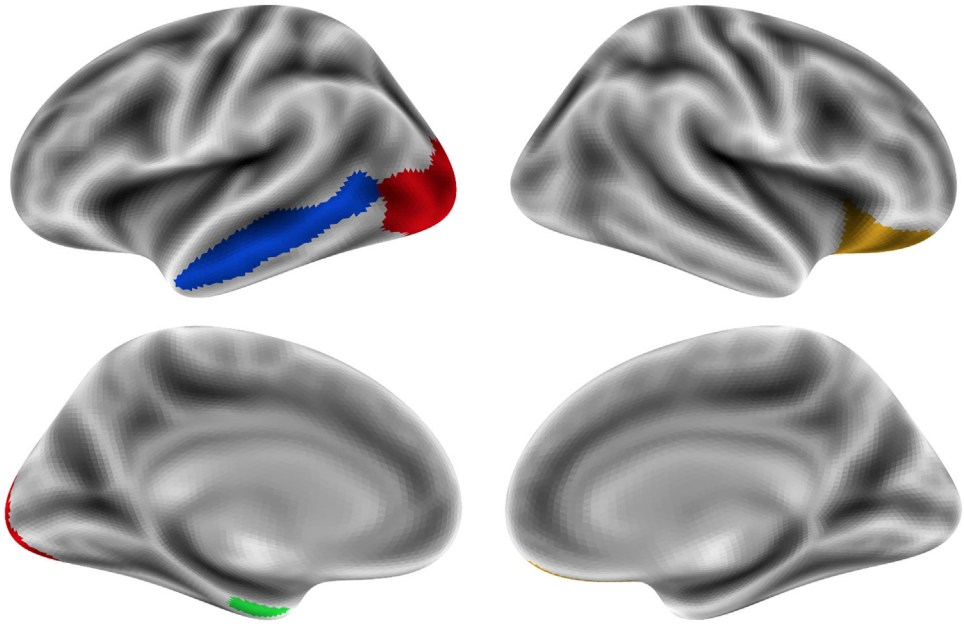

Fig. 4. Cortical fractal dimensionality parcels that exhibited unique significant effects on delay reward discounting area under the curve. Blue = Left Middle Temporal FD, Yellow = Right Lateral Orbitofrontal FD, Red = Left Lateral Occipital FD, Green = Left Entorhinal Cortex.

Table 3
Final hierarchical regression model with fractal dimensionality of parcellated cortical regions and sulcal morphology as predictors of an area under the curve discounting measure.

	F	*B*	*SE*	*t*	*p*	Δ Marginal R^2/ Combined Marginal R^2
Covariate Model						.023/.082
Sex	2.968	−0.032	0.019	−1.723	.085	–
Age	0.011	0.000	0.002	0.107	.915	–
Income	8.968	0.010	0.003	2.995	.003	–
Dizygotic Twin Status	0.109	0.007	0.020	0.331	.741	–
Monozygotic Twin Status	0.002	0.001	0.016	0.044	.965	–
Total Intracranial Volume	0.909	−0.010	0.011	−0.953	.340	–
Morphometry Indicators						.059/.082
L Middle Temporal Gyrus FD	8.987	1.060	0.354	2.998	.003	.022
L Lateral Occipital Cortex FD	8.399	1.030	0.355	2.898	.004	.012
R Inferior Frontal Sulcus Depth	6.984	0.011	0.004	2.643	.008	.010
L Entorhinal Cortex FD	5.858	0.448	0.185	2.420	.016	.008
L Central Sulcus Width	6.995	0.040	0.015	2.645	.008	.007

Note. *R*= Right. *L*= Left. OFC = Orbitofrontal Cortex. SE = Standard Error. Only regions with significant *p*-values after family-wise error correction are included ($p_{FWE} < 0.05$) Delay discounting was assessed using mean area under the curve for $200 and $40,000 tasks. Smaller area under the curve is indicative of higher delayed reward discounting.

Table 4
Final hierarchical regression model including sulcal morphology, fractal dimensionality, and gray matter volume of cortical parcels as predictors of an area under the curve discounting measure.

	F	*B*	*SE*	*t*	*p*	Δ Marginal R^2/ Combined Marginal R^2
Covariate Model						.023/.077
Sex	2.194	−0.027	0.019	−1.481	.139	–
Age	0.009	2.0E-4	0.002	0.096	.924	–
Income	9.603	0.010	0.003	3.099	.002	–
Dizygotic Twin Status	0.206	0.009	0.020	0.454	.650	–
Monozygotic Twin Status	0.001	−0.001	0.016	−0.035	.972	–
Total Intracranial Volume	0.777	−0.009	0.011	−0.882	.378	–
Morphometry Indicators						.054/.077
L Middle Temporal Gyrus FD	8.829	1.054	0.355	2.971	.003	.022
L Entorhinal GMV	8.689	6.5E-5	2.2E-5	2.948	.003	.014
L Lateral Occipital FD	7.117	0.011	0.004	2.668	.008	.009
R Inferior Frontal Sulcus Depth	8.829	1.054	0.355	2.971	.003	.009

Note. N = 973. FD = Fractal Dimensionality. L = Left. R = Right. GMV = Gray Matter Volume. Only regions with significant p-values after FWE correction are included ($p_{FWE} < 0.05$). Delay discounting was assessed using mean area under the curve for $200 and $40,000 tasks. Smaller area under the curve is indicative of higher delayed reward discounting.

ciated with less wide and more shallow sulci. These patterns may differ as participants included in the current study were young, healthy individuals, unlikely to exhibit age-related atrophy. Furthermore, the inclusion of age as a covariate of analysis should have also circumvented any age-related effects. Rather, these variations in SM may be due to genetic or environmental factors impacting neurodevelopment. Indeed, according to the tension-based theory of cortical folding, alterations in morphogenesis of the sulci during development are due to differing mechanical tension along axons within the subcortical white matter (Van Essen, 1997; Davatzikos et al., 2002). Further, in certain conditions such as Down's Syndrome, reduced average and regional sulcal depth have been observed in living fetuses, highlighting that sulcal alterations may occur during fetal development and their utility as neurocognition markers (Yun et al., 2021). While the effects of SM on cognition have not been explicitly studied to our knowledge, changes likely reflect reduced size or density of cells, which correlate to cognitive changes in certain conditions, such as multiple sclerosis (Liu et al, 2014). Interestingly, sulcal widening has been previously linked to lowered cognitive performance (Liu et al., 2011), however, in the current study, sulcal widening was associated with lower delay discounting. This conflicts with abundant research linking lowered delay discounting to increased cognitive ability (Shamosh and Gray, 2008). More research is warranted to delineate these relationships and to consider whether these links between alterations in SM and DRD preferences may represent biobehavioral variations that precede comorbid neurological and psychiatric conditions (e.g., ADHD, bipolar disorder, substance use disorder).

Analysis of FD revealed that of the 62 cortical parcels included, 15 were significantly associated with DRD after FWE correction, and 4 cortical predicted unique significant variance in DRD: 1) the left middle temporal gyrus, 2) the right lateral OFC, 3) left lateral occipital cortex, and 4) left entorhinal cortex. In all regions, lowered FD, or lowered complexity, was associated with heightened devaluation of future rewards. Of these findings, reduced FD of the left middle temporal gyrus, right lateral OFC, and left entorhinal cortex corresponded with our hypotheses. Contrary to our hypotheses, FD of the PCC did not any display unique significant contributions to DRD behavior.

FD of the left middle temporal gyrus accounted for the highest amount of unique variance in DRD. This finding was hypothesized given that Owens et al. (2017) found that GMV of the bilateral middle temporal gyri was negatively correlated with DRD and had unique significant effects on DRD preferences in the same dataset. This finding is further supported by MacKillop et al. (2012), who found associations between activity in the middle temporal gyrus and intertemporal choice decision-making in a preliminary functional MRI study including adult smokers. While DRD-specific literature regarding the middle temporal gyrus is limited, it is an established node within the default mode network wherein activity increases during goal-directed tasks involving self-generated thought, such as episodic information retrieval and future planning (Andrews-Hanna et al., 2014). Lowered FD in this region may relate to lower neuron density and less activation of this region during tasks; however, given structural findings do not always relate to functional findings, more research is required to discern what the effects of lowered FD, or complexity, of this region may beget. The association between FD of the entorhinal cortex also coincides with those of Owen's et al. (2017), wherein they found reduced GMV of the bilateral entorhinal cortex had unique significant contributions to DRD behavior. This finding is also supported Lempert et al. (2020) who found that decreased cortical thickness of the entorhinal cortex was associated with higher DRD in healthy aging adults and adults with mild cognitive decline. Further, Lempert et al. (2020) found that this effect was partially mediated by episodic memory and that rates of perception-based details in autobiographical memories were correlated with entorhinal CT. Taken together, these findings suggest the importance of the entorhinal cortex in vividly recalling past experiences to create representations of future scenarios; a process required to make rational DRD decisions.

The FD of the cortical parcel that predicted the second highest amount of unique variation in DRD preferences was the right lateral OFC. This finding was in line with our hypotheses, which were based on the role of the OFC in DRD decision-making in previous research. the link between the GMV of the right OFC and DRD has been previously demonstrated by Mohammadi et al. (2016), wherein they found that GMV of the right OFC was significantly associated with DRD rates within small samples of healthy controls and pathological gamblers. This finding was also observed by Owen's et al., (2017) who revealed that the GMV of the right and left lateral OFC was significantly associated with DRD preferences; however, unlike the current study, the OFC did not provide significant variance beyond the bilateral middle temporal gyrus and entorhinal cortex. This incongruity may be attributable to FD being a more sensitive measure of neuroanatomical variation than GMV, as was seen with cortical thickness and gyrification (Madan and Kensinger, 2016). Functionally, as the right OFC cortex plays a role in value-based decision making (Wallis, 2007), the observed FD deficits in this parcel may be associated with problematic valuation leading to heightened DRD. The final cortical parcel wherein FD predicted DRD behavior was the lateral occipital cortex. This finding is unexpected given it has not been seen in previous structural DRD literature and as the primary function of the lateral occipital cortex is believed to be object recognition (Grill-Spector et al., 2001). Of note, Hare et al. (2014) did find significant activation of the occipital cortex during delayed reward selection after whole-brain correction. Further research controlling for

visual stimuli is required to discern whether the lateral occipital cortex is truly related to DRD behavior.

Whether FD differences in these regions are due to local atrophy or developmental alterations is unclear within the scope of the current study. While alterations in FD are often attributed to atrophy (Collantoni et al., 2020; Madan and Kensinger, 2016; King et al., 2010), Esteban et al. (2009) found that reductions in whole-brain FD in multiple sclerosis patients were not correlated with GM atrophy. Furthermore, research has demonstrated that surface-based morphometry, such as cortical FD, generally develop until early childhood, at which point the morphology becomes more stable (Armstrong et al., 1995). Under this logic, local FD alterations may occur during development and may be antecedents to steep DRD and comorbid psychopathologies. Further research is required to improve understanding the origins of cortical FD alterations and how they relate to DRD. While research involving FD is still limited, literature has shown a significant positive relationship between FD across the right hemisphere and IQ . Given the relationship between DRD and IQ (Bailey et al., 2020), it may be valuable to explore whether IQ may modulate the relationship between FD and DRD. When considering the location of cortical parcels that demonstrated unique significant contributions to DRD preferences, parcels spanned the temporal lobe (i.e., left middle temporal gyrus and left entorhinal), frontal lobe (i.e., right lateral orbitofrontal), and occipital lobe (i.e., left lateral occipital). Contrastingly, findings in the literature predominantly implicate cortical alterations within the frontal lobe (Cho et al., 2015; Wang et al., 2016; Bjork et al., 2009; Drobetz et al., 2014). The lack of existing structural findings within the temporal and occipital lobes may be due to several of these studies limiting analysis to a priori ROIs, possessing minimal sample sizes, and utilizing incongruent DRD tasks, scanner resolution and sample ages.

When considering SM and FD of cortical parcels simultaneously, results revealed that including both indicators in the model accounted for more unique variance in DRD preferences than SM or FD alone. Further, the FD of the right lateral OFC FD no longer provided significant unique variance, indicating that SM and FD are capturing some degree of common variance. When repeating the integrated analysis including the two bilateral GMV regions that had significant unique effects on DRD preferences (i.e., bilateral MTG and entorhinal cortex) within the same sample by Owens et al. (2017), all significant regions remained the same except the FD of the entorhinal cortex which was replaced by the GMV of the entorhinal cortex and removal of the left central sulcus width. In addition, rather than accounting for the least amount of unique variance in the model, GMV of the entorhinal cortex accounted for the second-highest amount of unique variance in DRD preferences. These results indicate that, when assessing changes in entorhinal cortex morphology in relation to DRD preferences, GMV may capture further variation than FD. Beyond variance explained by covariates in the model, Owens et al., (2017) found that using GMV of cortical parcels accounted for 4.2% of unique variance in DRD preferences. When rerunning these through the mixed-effect hierarchical regression model used in the current study, this was reduced to 3.6%. In the current study, all models except for SM only exceeded this, with FD predicting 4.7%, SM and FD predicting 5.9%, and SM, FD, and GMV predicting 5.4%. Taken together, these findings fulfill our third hypothesis and demonstrate the utility of FD and SM morphometry indicators to capture the complex patterns of morphology that underlie DRD. When comparing FD and GMV and FD and CT of the same parcels, shared variance ranged from 24.3% to 85.7% with a median shared variance of 66.6% and 4.7% to 38.0% with a median shared variance of 16.3%, respectively. These results indicate that, while there is some degree or overlap, there is a substantial amount of unique variance explained by this novel measure.

Several considerations bear on the current results. First, given that this was the first investigation of SM and FD in relation to DRD, it was exploratory and tested a large the number of regions, increasing risk of type I error. While, FDR correction and a large sample size were employed to mitigate these risks, future studies should utilize these results to inform a priori regions, allowing a hypothesis-driven approach. In addition, reward choices in the study were hypothetical, leading to responses that may not accurately reflect real-life decisions. However, a number of studies have shown high correspondence between choices for hypothetical and actual DRD outcomes (Madden et al., 2003; Amlung et al., 2012). Considering the sample, the current study also lacked racial diversity. Accordingly, future research would benefit from a more diverse sample to improve the generalizability of the results. Finally, as the study was cross-sectional, causation cannot be inferred. Thus, for a better understanding of whether these neuroanatomical alterations precede the development of steepened DRD, further research should address this question longitudinally. Acknowledging these considerations, the study also had numerous strengths including a very large sample size, a relatively high-resolution DRD phenotype, and a systematic analytic strategy. In addition, as the sample was composed of young healthy individuals, the observed neuroanatomical alterations are not likely to due to disease-, substance-, or age-related atrophy, and thus are more likely to reflect alterations derived during development that precede the DRD behavioral phenotype.

While advancements have been made in understanding the neuroanatomical variations that underlie DRD, inconsistent findings underscore the need for large sample sizes to discover reproducible associations between brain structure and behavioral phenotypes such as DRD (Marek et al., 2020). In a large (n = 1038) sample of healthy, young adults from the HCP dataset, results of the current study implicate local reductions in cortical complexity and increased sulcal width and depth across the frontal, occipital, and temporal lobes as morphological substrates of steepened DRD. Further, they affirm that SM and FD are able to capture the complex cortical patterns that underlie DRD. In fact, results reveal FD to be a more sensitive measure of DRD-related cortical alterations than GMV, a common structural indicator, in all nearly all implicated cortical parcels. As the first study to consider FD and SM in relation to DRD, the current study lays groundwork for future research to further elucidate the neuroanatomical underpinnings of DRD employing a hypothesis-driven approach. Together with the current results, this may offer the potential to enhance understanding of steepened DRD and delineate its relationships with several neurological conditions, such as bipolar disorder, substance use disorder, and schizophrenia.

4. Methods

4.1. Participants

Participants were drawn from a community sample of 1206 individuals recruited through the Human Connectome Project (HCP), a large open access study that aimed to map the human connectome in healthy young adults. Eligible individuals were between the ages of 22 and 35 with the goal of providing a sample that had passed major neuromaturation benchmarks but was prior to the onset of potential neurodegeneration (Van Essen et al., 2012). Exclusion criteria included genetic disorders, significant head injuries, contraindications to MRI (e.g., pregnancy, unsafe metal devices or claustrophobia), and significant history of psychiatric disorder, substance use, or neurological and cardiovascular disease. All participants provided informed consent and research was completed in accordance with the Declaration of Helsinki. Detailed explanations regarding the inclusion and exclusion criteria and informed consent are available elsewhere (Van Essen et al., 2013). Recruitment, consent, and sharing of data protocols were approved by the Washington University Institutional Review Board. No further ethical review was completed.

Of the 1206 individuals in the original study, 1113 underwent structural MRI scans and were included in the present study. Of those, a further 75 participants were excluded: 8 due to missing DRD data, 65 due to inconsistent DRD data (see quality control procedures below), and 2 due to missing income values. As displayed in Table 5, the full final sample included 1038 individuals that were, on average, in their late

Table 5
Comparison of full sample participant characteristics and complete SM data.

Demographic Characteristic	M [SD] or%	M [SD] or%
	Full Sample[a]	Complete SM Data Only[b]
Age	28.86 [3.69]	28.82 [3.70]
Sex (% Female)	54.7	54.7
Race (% Caucasian)	75	74.7
Ethnicity (% Non-Hispanic)	90.4	89.7
Median Income (USD)	50,000 –74,999	50,000 –74,999
Years of Education	14.94 [1.80]	14.91 [1.81]

Note.[a]n =1038. [b]n=973. SM = Sulcal Morphology. *M* = Mean. SD = Standard Deviation. USD = U.S. Dollars.

twenties with a median household income of $50,000 to $74,999 USD and a modest overrepresentation of females (45.3% male). For analyses involving SM, a further 65 individuals were excluded due to missing at least one SM measure (e.g., left central sulcus width). This occurs if the toolbox cannot reliably determine the width or depth of a specific sulci (Madan, 2019). A comparison of the full sample and complete SM sample is available in Table 5.

4.2. Delayed reward discounting

Participants completed two DRD tasks to assess their affinity for smaller more proximal rewards over larger delayed rewards. Within each task, participants were asked to make a series of hypothetical choices between a varying immediate monetary reward and a fixed delayed reward (either $200 or $40,000 maximum) available after 1 month, 6 months, 1 year, 3 years, 5 years, and 10 years. The immediate monetary reward that was offered to participants was based on a previously validated adaptive adjusting amount procedure (Estle et al., 2006; Green et al., 2007), wherein the value of the present reward is adjusted based on the participant's previous response. For example, during the first trial, participants must choose between either $100 today or $200 in 1 month. If the participant selects the immediate reward, the subsequent immediate reward option will be reduced by half and they will be offered $50 today or $200 in 1 month. According to DRD theory, an individual's subjective value of a reward decreases as the reward becomes more remote (Mazur, 1987). Accordingly, by adjusting the magnitude of the immediate reward, the monetary amount at which the value of the present reward equals the participant's subjective value of the larger delayed reward can be quantified and labelled as the point of indifference (POI). This procedure was repeated for both maximum delayed rewards ($200 and $40,000) at each delay length (1 month, 6 months, 1 year, 3 years, 5 years, and 10 years), for a total of 12 combinations.

To ensure adequate attention was given to DRD tasks, a quality control procedure was implemented in each following a previously established technique (Owens et al., 2017). Using the POIs for each delay length on both the $200 and $40,000 DRD task, each participant was assessed for response consistency. Across each task, if the POI remained the same between delay lengths or increased in magnitude, it was counted as an inconsistency. If, across the six POIs in each task, the participant had more than three inconsistencies, they were removed from the study. For example, if a participant had a POI of $96.88 at the 1-month delay for the $200 DRD task and had a POI of $103.13 at the 6-month delay, that would be counted as one inconsistency. This follows the principles of temporal discounting which ascertain that the subjective value of the reward decreases with increased delay (Myerson et al., 2001; Green et al., 2007). The implementation of this quality control measure resulted in the removal of 65 additional participants (5.8% of the original sample).

The POIs from the $200 and $40,000 DRD tasks were each concatenated into a single discounting variable referred to as an area under the curve (AUC) discounting measure (Myerson et al., 2001). A smaller AUC is representative of steeper discounting of delayed rewards. AUC values for the $200 and $40,000 DRD tasks were normally distributed and were found to be moderately correlated ($r = .668$, $p = 2.4E\text{-}135$); as a result, a mean AUC (mAUC) value was calculated for each participant.

4.3. Structural MRI acquisition

4.3.1. Scanning protocol

Participants were scanned within a 2-day span between August 2012 and October 2015 using a custom Siemens Skyra 3T scanner with a 32-channel head coil (Siemans AG. Erlanger, Germany) at Washington University, St. Louis. Two 7-minute T1-weighted (T1w) and two 8-minute T2-weighted (T2w) 0.7 mm isotropic structural scans were obtained per participant. The parameters for the T1 scans were field of view (FOV) = 224 mm x 224 mm, matrix = 320, 256 sagittal slices, repetition time (TR) = 2400 ms, echo time (TE) = 2.14 ms, inversion time (TI) = 1000 ms, flip angle (FA) = 8°, and bandwidth (BW) = 210 Hz/pixel. The parameters for the T2 scans were FOV = 224 mm x 224 mm, matrix = 320, 256 sagittal slices, TR = 3200 ms, TE = 565 ms, TI = variable, and BW = 744 Hz/pixel. If technical issues were encountered or if the quality of the scans was deemed inadequate, the participants underwent an additional scanning session. The quality of structural scans was inspected and rated by an experience rater based on criteria including tissue contrast, presence of motion artifacts, ringing, blurriness, and abnormal anatomy. To be included in the HCP data release, participants were required to have a minimum of one T1w and one T2w scan that received a rating of "good" or higher within the same scan session.

4.3.2. Preprocessing

HCP structural MRI preprocessing relevant to the current study can be broken down into three pipelines: 1) PreFreeSurfer, 2) FreeSurfer, and 3) Local Gyrification Index. All steps were designed to account for the high spatial and temporal resolution of images and to retain maximum data by limiting processing. An in-depth explanation of each step is described elsewhere (Glasser et al., 2013). Briefly, the objectives of the PreFreeSurfer pipeline included creating an undistorted "native" space for within subject structural data. This included gradient distortion correction necessitated by the unique design of the HCP Skyra scanner, alignment and averaging of T1w and T2w images if more than one quality image (see Scanning Protocol) was obtained per participant, and rigid alignment of T1w and T2w images to the MNI space template (with 0.7 mm resolution). Additionally, T1w and T2w images underwent field bias correction and T1w images were registered to MNI space to allow for comparisons across subjects and studies, particularly for subcortical data (Glasser et al., 2013). Two output folders were produced; one with all images in native volume space and another with all images registered to MNI space.

The FreeSurfer step was the use of an adapted version of the FreeSurfer v5.3.0 main processing stream "recon-all" which has been widely used in MRI studies for the quantification of neuroanatomical structures (Fischl, 2012; https://surfer.nmr.mgh.harvard.edu/fswiki/recon-all). The undistorted, bias-corrected T1w image (i.e., native volume space) output from the PreFreeSurfer pipeline served as the input. As recon-all has been developed to run with 1 mm isotropic resolution scans, the 0.7 mm isotropic HCP scans were first downsampled to 1 mm isotropic resolution with spline interpolation (Glasser et al., 2013). The majority of the recon-all pipeline was then permitted to run, including segmentation of neuroanatomical structures (Fischl et al., 2002) and tessellation and removal of topological defects of the white matter surface (Dale et al., 1999). The recon-all pipeline was interrupted when the final white matter surfaces were generated and 1.0 mm downsampled scans were returned and readjusted in the 0.7 mm native volume space (see Glasser et al., 2013 for more details). Images were returned to 1.0 mm resolution and the final steps of the recon-all pipeline were completed which included inflation of white matter surfaces (Fischl et al., 1999a), surface-based registration to the FreeSurfer

average template to increase the accuracy of alignment to major sulcal and gyral landmarks (Fischl et al., 1999b), and sulcal and gyral segmentation (Destrieux et al., 2010). Recon-all was then halted and pial surfaces were identified through an improved algorithm that utilised both the high-resolution T1w and T2w images. The recon-all pipeline then recommenced and the final steps, including cortical parcellation and volumetric and surface area quantification, were completed.

To prepare MRI data for SM quantification, the pial output from the recon-all pipeline (h.pial) was processed through an additional script, Local Gyrification Index (Schaer et al., 2008; https://surfer.nmr.mgh.harvard.edu/fswiki/LGI). This processing stream creates a smoothed outer surface that tightly wraps the pial surface and uses it to create a ratio with each vertex of the pial surface within three-dimensional (3D) regions of interest. The final output files include ".pial-outer-smoothed" which is used as an input for the generation of SM and FD measurements.

4.4. Sulcal morphology

Sulcal morphology was employed as a measure to assess the width and depth of several sulci of the brain. Measurements were obtained via the validated MATLAB toolbox *calcSulc* (Madan, 2019), which bases calculations on the cortical reconstruction (?h.pial), parcellation (h.aparc.a2009.annot), and sulcal map (?h.sulc) outputs of the FreeSurfer recon-all pipeline along with the "?h.pial-outer-smoothed" output from the local gyrification analysis (Madan, 2019; https://cmadan.github.io/calcSulc/). Cortical parcellation was based on the Destrieux et al., atlas which is included within the standard recon-all pipeline (Destrieux et al., 2010). The toolbox produces estimates of bilateral sulcal widths and depths in eight major sulci of the brain: 1) occipito-temporal, 2) middle occipital and lunate, 3) parieto-occipital, 4) post-central, 5) marginal part of the cingulate, 6) central, 7) superior frontal, and 8) inferior frontal (32 measurements total). The width measurement is calculated by marking the vertices at the boundary between the gyrus and the sulcus on both sides and then finding the shortest distance between each boundary vertex and a vertex on the opposite side. The sulcal depth is similarly calculated by identifying vertices at the fundus of the sulcus and finding the shortest distance between each vertex of the fundus and a vertex on the enclosing surface of the sulcus. The measurement reliability of this toolbox has been validated using test-retest data (Madan, 2019) and intraclass correlation coefficients (ICC) which indicated excellent reliability for all sulcal depth (ICC = .848 - .979) and sulcal width (ICC = .757 - .864) measurements, except for widths of the bilateral parieto-occipital, occipito-temporal, and middle occipital and lunate sulci which indicated good reliability (ICC = .605 - .692).

4.5. Fractal dimensionality

FD was employed as a measure to assess the structural complexity of parcellated cortical and segmented subcortical 3D structures of the brain. FD measurements were obtained via the validated MATLAB toolbox *calcFD*, which bases calculations on cortical reconstruction and parcellation outputs from the FreeSurfer recon-all pipeline, including "ribbon.mgz" and "aparc.a2009s+aseg.mgz", and local gyrification index outputs (Madan and Kensinger, 2016; http://cmadan.github.io/calcFD/). To assess FD, a select neuroanatomical structure on an MRI image is overlayed with a grid of boxes of a particular size (e.g., 2 mm). The number of boxes that contain either the border (i.e., surface-only) or filled space within (i.e., filled volume) the structure of interest (e.g., hippocampus) are counted. The box size can be then increased, either on a fixed grid (box-counting method) or on a sliding grid scale (dilation method), and the boxes containing the structure are counted again. Fractal dimensionality is then quantified as the negative double logarithmically transformed change in the number of cubes containing the structure over change in cube size ($FD = -\frac{\Delta log2(Count)}{\Delta log2(Size)}$). Put another way, FD represents the steepness of the gradient by which increasing cube size reduces the number of cubes required to fully capture a structure. This measure captures complexity as more complex structures show greater reductions in the number of cubes required to capture them as cube size grows, owing to the larger number of cubes needed at high resolutions to capture higher complexity. The current study used the filled volume method with 1 mm, 2 mm, 4 mm, 8 mm, and 16 mm cubes and the dilation algorithm. These options were selected as filled volume has been shown to yield improved measurement of age-related differences (Esteban et al., 2009) and the dilation algorithm has been shown to yield superior measurements compared to the box-counting method (Madan and Kensinger, 2016; Madan and Kensinger, 2017). FD was calculated for all cortical regions included in the DKT atlas with the exception of the banks of the superior temporal sulcus, the corpus callosum, and the frontal and temporal poles, resulting in 31 cortical regions per hemisphere. The FD of 7 subcortical structures was also assessed based on segmentation using the conventional FreeSurfer subcortical segmentation protocol (Fischl et al., 2002).

4.6. Data analysis

4.6.1. Correlational analysis

Before beginning the primary analysis, associations between bilateral SM and FD measures were explored using zero-order correlations. Additionally, partial correlations were used to determine the magnitude of association between SM and FD regions and mAUC, including sex, age, income, intracranial volume, and monozygotic and dizygotic twin status as covariates. Partial correlations were then FWE corrected using a permutation analysis and were ranked based on corrected *p*-values within three subgroups: 1) SM regions, 2) FD of cortical parcels, and 3) SM regions and FD of cortical parcels combined. Finally, to permit comparison with findings from a study that explored DRD and GMV of cortical parcels in the same dataset (Owens et al., 2017), partial correlations were ran between GMV of parcels previously found to be significant predictors of mAUC – the GMV of the bilateral entorhinal cortex and MTG. These partial correlations were then FWE corrected and ranked alongside SM and FD indicators in a fourth subgroup.

4.6.2. Permutation analysis

In addition to partial correlation analyses, to account for the unusual variance structure of the HCP dataset (i.e., substantial inclusion of siblings) and to correct for FWE, we used a permutation testing approach to evaluate the association between each brain metric and DRD. Associations were quantified by the Aspin-Welch *v* score, an alternative to a t-score that better accounts for heteroscedasticity. The same covariates as the partial correlation analyses were used in permutation testing. This approach was implemented in the Python library Neurotools (https://github.com/sahahn/neurotools), using an exchangeability block approach analogous to that of PALM software (Winkler et al., 2014; https://fsl.fmrib.ox.ac.uk/fsl/fslwiki/PALM). In this approach, a null distribution was created by conducting 10,000 permutations, in which DRD labels were shuffled and the association between each brain metric and the shuffled DRD score was assessed. To maintain the variance structure of the original data, the label shuffling was performed according to two constraints:

1. Swaps were permitted to occur between entire families of the same size. For example, for a family of size two, a valid swap would involve switching their labels with both members of another family of size two. On the other hand, all singletons were allowed to freely swap with any other singleton.
2. Swaps were permitted within family, that is, any two siblings could freely exchange labels with each other.

To correct for multiple comparisons, the maximum *v*-score among all brain metrics was identified from each of the 10,000 permutations. These were used to create a distribution of max *v*-scores under the

null hypothesis (i.e., a distribution of the largest scores likely to occur by chance in a given family of tests). After creating this null distribution, an Aspin-Welch *v* score was calculated for the actual association of each brain metric and DRD, and the *p*-value of that score was determined using the null distribution. Thus, for each brain region, an Aspin-Welch *v* score and family-wise error (FWE) corrected *p*-value were generated.

4.6.3. Linear mixed effects modeling

SM and FD regions that were significantly correlated with mAUC and survived FWE correction were further analyzed to ascertain which had unique effects on mAUC. Given the HCP dataset is comprised of siblings, linear mixed effect modeling was conducted to account for differences which may be attributable to shared experience and genetics as opposed to neuroanatomical differences. All models were completed with family as a random intercept; mAUC as the dependant variable; sex, dizygotic twin status, and monozygotic twin status as factors; and income, age, and intracranial volume as scale variables. For the first step, SM regions that were significantly correlated with mAUC were added to the model based on order of correlation magnitude with mAUC. If the region was a significant predictor of mAUC, it remained in the subsequent model as a scale variable and the next highly correlated region was added to the model. If the region was not a significant predictor, it was removed from the model and the next highly correlated region was added. This process was completed iteratively for all SM regions until a final model was established. The same iterative modeling process was then completed for all FD regions, SM and FD regions combined, and SM, FD, and GMV regions combined. All correlational and mixed effect models were completed using SPSS (Version 26).

To improve interpretability of results and to permit better comparison between models in the current study and in Owens et al. (2017), coefficient of determination (R^2) values were generated for each final model. As R^2 is not readily available in linear mixed-effects models, all final mixed effect models were reproduced in R studio (version 1.4.1103) and R^2 values were calculated using the R package r2_nakagawa (Nakagawa and Schielzeth, 2012). The output includes values for marginal and conditional R^2, wherein marginal R^2 estimates variance of the fixed effects (i.e., covariates and morphological indicators) as a proportion of all variance and conditional R^2 includes variance explained by the random effects (i.e., family groupings) and fixed effects.

Credit statement

Carly McIntyre-Wood: Conceptualization, Methodology Formal analysis, Writing - Original Draft

Christopher Madan: Methodology Software Formal analysis, Review & Editing

Max Owens: Formal analysis, Methodology Review & Editing

Michael Amlung: Conceptualization, Review & Editing

Lawrence H. Sweet: Conceptualization, Review & Editing

James MacKillop: Conceptualization, Methodology, Writing - Review & Editing, Supervision

Data and code availability statement

Delay reward discounting data and 3T MR imaging data were obtained from the WU-Minn HCP Consortium open access 1200 Subjects Data Release (see https://www.humanconnectome.org/study/hcp-young-adult) in accordance with the HCP Data Use Terms.

Declaration of Competing Interest

James MacKillop is a principal in BEAM Diagnostics, Inc. and a Consultant to Clairvoyant Therapeutics; no other authors have potential conflicts of interest to disclose.

Funding and Acknowledgements

All data were provided by the Human Connectome Project, WU-Minn Consortium (Principal Investigators: David Van Essen and Kamil Ugurbil; 1U54MH091657) funded by the 16 NIH Institutes and Centers that support the NIH Blueprint for Neuroscience Research; and by the McDonnell Center for Systems Neuroscience at Washington University in St. Louis. The authors are grateful to the Human Connectome Project for open access to its data. The current work using the Human Connectome Project data was supported by the Peter Boris centre for Addictions Research. The funding source had no role in the study design, execution, or manuscript preparation. The authors thank Sage Hahn for providing helpful consultation regarding permutation testing analyses.

Supplementary materials

Supplementary material associated with this article can be found, in the online version, at doi:10.1016/j.neuroimage.2022.119309.

References

Amlung, M.T., Acker, J., Stojek, M.K., Murphy, J.G., MacKillop, J., 2012. Is talk "cheap"? An initial investigation of the equivalence of alcohol purchase task performance for hypothetical and actual rewards. Alcohol Clin. Exp. Res. 36 (4), 716–724. doi:10.1111/j.1530-0277.2011.01656.x.

Amlung, M., Petker, T., Jackson, J., Balodis, I., Mackillop, J., 2016. Steep discounting of delayed monetary and food rewards in obesity: a meta-analysis. Psychol. Med. 46 (11), 2423–2434. doi:10.1017/S0033291716000866.

Amlung, M., Vedelago, L., Acker, J., Balodis, I., MacKillop, J., 2017. Steep delay discounting and addictive behavior: a meta-analysis of continuous associations. Addiction 12 (1), 51–62. doi:10.1111/add.13535.

Andrews-Hanna, J.R., Smallwood, J., Spreng, R.N., 2014. The default network and self-generated thought: component processes, dynamic control, and clinical relevance. Ann. N Y Acad. Sci. 1316 (1), 29–52. doi:10.1111/nyas.12360.

Armstrong, E., Schleicher, A., Omran, H., Curtis, M., Zilles, K., 1995. The ontogeny of human gyrification. Cereb Cortex 5 (1), 56–63. doi:10.1093/cercor/5.1.56.

Aron, A., Robbins, T., Poldrack, R., 2014. Inhibition and the right inferior frontal cortex: one decade on. Trends Cogn Sci. 18 (4), 177–185. doi:10.1016/j.tics.2013.12.003.

Baddeley, A., 1992. Working Memory. Science 255 (5044), 556–559. doi:10.1126/science.173635.

Bailey, J.A., Gerst, K., Finn, R.P., 2020. Intelligence moderates the relationship between delay discounting rate and problematic alcohol use. Psychol Addict Behav 34 (1), 175–181. doi:10.1037/adb0000471.

Bertoux, M., et al., 2019. Sulcal morphology in Alzheimer's disease: an effective marker of diagnosis and cognition. Neurobiol Aging 84, 41–49. doi:10.1016/j.neurobiolaging.2019.07.015.

Bickel, W.K., Jarmolowicz, D.P., Mueller, E.T., Koffarnus, M.N., Gatchalian, K.M., 2012. Excessive discounting of delayed reinforcers as a trans-disease process contributing to addiction and other disease-related vulnerabilities: emerging evidence. Pharmacol. Ther. 134 (3), 287–297. doi:10.1016/j.pharmthera.2012.02.004.

Bickel, W.K., Miller, M.L., Yi, R., Kowal, B.P., Lindquist, D.M., Pitcock, J.A., 2007. Behavioral and neuroeconomics of drug addiction: competing neural systems and temporal discounting processes. Drug Alcohol Depend. 90 (Suppl 1), S85–S91. doi:10.1016/j.drugalcdep.2006.09.016.

Bickel, W.K., Yi, R., Landes, R.D., Hill, P.F., Baxter, C., 2011. Remember the future: working memory training decreases delay discounting among stimulant addicts. Biol. Psychiatry 69 (3), 260–265. doi:10.1016/j.biopsych.2010.08.017.

Bjork, J.M., Momenan, R., Hommer, D.W., 2009. Delay discounting correlates with proportional lateral frontal cortex volumes. Biol. Psychiatry 65 (8), 710–713. doi:10.1016/j.biopsych.2008.11.023.

Cai, K, et al., 2017. Identification of early-stage Alzheimer's Disease using sulcal morphology and other common neuroimaging indices. PLoS One. 12 (1), e0170875. doi:10.1371/journal.pone.0170875.

Chib, V.S., Rangel, A., Shimojo, S., O'Doherty, J.P, 2009. Evidence for a common representation of decision values for dissimilar goods in human ventromedial prefrontal cortex. J. Neurosci. 29 (39), 12315–12320. doi:10.1523/JNEUROSCI.2575-09.2009.

Cho, S.S., Koshimori, Y., Aminian, K., Obeso, I., Rusjan, P., Lang, A.E., Daskalakis, Z.J., Houle, S., Strafella, A.P., 2015. Investing in the future: stimulation of the medial prefrontal cortex reduces discounting of delayed rewards. Neuropsychopharmacology 40 (3), 546–553. doi:10.1038/npp.2014.211.

Cho, S.S., Pellecchia, G., Aminian, K., Ray, N., Segura, B., Obeso, I., et al., 2013. Morphometric correlation of impulsivity in medial prefrontal cortex. Brain Topogr. 26, 479–487. doi:10.1007/s10548-012-0270-x.

Coffey, E.C., et al., 1992. Quantitative cerebral anatomy of the aging human brain: A cross-sectional study using magnetic resonance imaging. Neurology 42 (3), 527–536. doi:10.1212/WNL.42.3.527.

Collantoni, E., Madan, C.R., Meneguzzo, P., Chiappini, I., Tenconi, E., Manara, R., Favaro, A., 2020. Cortical complexity in anorexia nervosa: a fractal dimension analysis. J. Clin. Med. 9 (3), 833. doi:10.3390/jcm9030833.

Dale M, A, Fischl, M, Sereno I, M, 1999. Cortical surface-based analysis. I. Segmentation and surface reconstruction. Neuroimage 9 (2), 179–194. doi:10.1006/nimg.1998.0395.

Davatzikos, C., Bryan, R.N., 2002. Morphometric analysis of cortical sulci using parametric ribbons: a study of the central sulcus. J. Comput .Assist Tomogr. 26 (2), 298–307. doi:10.1097/00004728-200203000-00024.

Demanet, J., Liefooghe, B., Hartstra, E., Wenke, D., De Houwer, J., Brass, M., 2016. There is more into 'doing' than 'knowing': the function of the right inferior frontal sulcus is specific for implementing versus memorising verbal instructions. Neuroimage 141, 350–356. doi:10.1016/j.neuroimage.2016.07.059.

Destrieux, C., Fischl, B., Dale, A., Halgren, E., 2010. Automatic parcellation of human cortical gyri and sulci using standard anatomical nomenclature. Neuroimage 53 (1), 1–15. doi:10.1016/j.neuroimage.2010.06.010.

Dixon, M.R., Marley, J., Jacobs, E.A., 2003. Delay discounting by pathological gamblers. J. Appl. Behav. Anal. 36 (4), 449–458. doi:10.1901/jaba.2003.36-449.

Drayer, P.B., 1988. Imaging of the aging brain. Part I. Normal findings. Radiology. 166, 785–796. doi:10.1148/radiology.166.3.3277247.

Drobetz, R., Hänggi, J., Maercker, A., Kaufmann, K., Jäncke, L., Forstmeier, S., 2014. Structural brain correlates of delay of gratification in the elderly. Behav. Neurosci. 128 (2), 134–145. doi:10.1037/a0036208.

Esteban, F.J., Sepulcre, J., de Miras, J.R., Navas, J., de Mendizábal, N.V., Goñi, J., Quesada, J.M., Bejarano, B., Villoslada, P., 2009. Fractal dimension analysis of grey matter in multiple sclerosis. J. Neurol. Sci. 282 (1–2), 67–71. doi:10.1016/j.jns.2008.12.023.

Estle, J.S., Green, L., Myerson, J., et al., 2006. Differential effects of amount on temporal and probability discounting of gains and losses. Mem Cognit 34, 914–928. doi:10.3758/BF03193437.

Figner, B., Knoch, D., Johnson, J.E., Krosch, R.A., Lisanby, H.S., Fehr, Ernst, Weber, U.E., et al., 2010. Lateral prefrontal cortex and self-control in intertemporal choice. Nat Neurosci. 13 (5), 538–539. doi:10.1038/nn.2516.

Finn, P.R., Gunn, R.L., Gerst, K.R., 2015. The effects of a working memory load on delay discounting in those with externalizing psychopathology. Clin. Psychol. Sci. 3 (2), 202–214. doi:10.1177/2167702614542279.

Fischl, B., 2012. FreeSurfer. Neuroimage 62 (2), 774–781. doi:10.1016/j.neuroimage.2012.01.021.

Fischl, B., Salat, H.D., Busa, E., Albert, M., Dieterich, M., Haselgrove, C., van der Kouwe, A., Killiany, R., Kennedy, D., Klaveness, S., Montillo, A., Makris, N, Rosen, B., Dale M., A., 2002. Whole brain segmentation: automated labeling of neuroanatomical structures in the human brain. Neuron. 33 (3), 341–355. doi:10.1016/s0896-6273(02)00569-x.

Fischl, B., Sereno, I.M., Dale, M.A., 1999. Neuroimage 9 (2), 195–207. doi:10.1006/nimg.1998.0396.

Fischl, B., Sereno, I.M., Tootell, H.R., Dale, A., 1999. High-resolution intersubject averaging and a coordinate system for the cortical surface. Hum Brain Mapp 8 (4), 272–284. doi:10.1002/(SICI)1097-0193(1999)8, 4<272::AID-HBM10>3.0.CO;2-4 PMCID: PMC6873338 PMID: 10619420.

Glasser, M., et al., 2013. The minimal preprocessing pipelines for the Human Connectome Projec. Neuroimage 80, 105–124. doi:10.1016/j.neuroimage.2013.04.127.

Green, L., Myerson, J., Shah, A., Estle, S., Holt, D., 2007. Do adjusting-amount and adjusting-delay procedures produce equivalent estimates of subjective value in pigeons? J Exp Anal Behav 87 (3), 337–347. doi:10.1901/jeab.2007.37-06.

Grill-Spector, K., Kourtzi, Z., Kanwisher, N., 2001. The lateral occipital complex and its role in object recognition. Vision Res 41 (10–11), 1409–1422. doi:10.1016/s0042-6989(01)00073-6.

Grizzi, F., Ceva-Grimaldi, G., Dioguardi, N., 2001. Fractal geometry: a useful tool for quantifying irregular lesions in human liver biopsy specimens. Ital. J. Anat. Embryol. 106 (2 Suppl 1), 337–346.

Guenther, F.H., Tourville, J.A., Bohland, J.W., 2015. Speech production. In: Brain Mapping. Academic Press, pp. 135–444. doi:10.1016/B978-0-12-397025-1.00265-7.

Hamelin, L., et al., 2015. Sulcal morphology as a new imaging marker for the diagnosis of early onset Alzheimer's disease. Neurobiol Aging 36 (11), 2932–2939. doi:10.1016/j.neurobiolaging.2015.04.019.

Hare, T., Hakimi, S., Rangel, A., 2014. Activity in dlPFC and its effective connectivity to vmPFC are associated with temporal discounting. Front Neurosci. 8, 50.

Horan, W.P., Johnson, M.W., Green, M.F., 2017. Altered experiential, but not hypothetical, delay discounting in schizophrenia. J. Abnorm. Psychol. 126 (3), 301–311. doi:10.1037/abn0000249.

Jackson, J.N., MacKillop, J., 2016. Attention-deficit/hyperactivity disorder and monetary delay discounting: a meta-analysis of case-control studies. Biol. Psychiatry 1 (4), 316–325. doi:10.1016/j.bpsc.2016.01.007.

Jin, K., Zhang, T., Shaw, M., Sachdev, P., and Cherbuin, N. (2018). Relationship Between Sulcal Characteristics and Brain Aging. *Front Aging Neurosci*, 10, 339. https://doi.org/10.3389/fnagi.2018.00339

Jackson, J.N.S., Mackillop, J., 2016. Attention-deficit/hyperactivity disorder and monetary delay discounting: a meta-analysis of case-control studies. Biol Psychiatry 1 (4), 316–325. doi:10.1016/j.bpsc.2016.01.007.

Kable, J., Glimcher, P., 2007. The neural correlates of subjective value during intertemporal choice. Nat Neurosci 10 (12), 1625–1633. doi:10.1038/nn2007.

King, R.D., Brown, B., Hwang, M., Jeon, T., George, A.T., 2010. Fractal dimension analysis of the cortical ribbon in mild Alzheimer's disease. Neuroimage 53 (2), 471–479. doi:10.1016/j.neuroimage.2010.06.050.

Koechlin, E., 2011. Frontal pole function: what is specifically human? Trends Cogn Sci. 15 (6), 241. doi:10.1016/j.tics.2011.04.005.

Lempert, K., et al., 2020. Neural and behavioral correlates of episodic memory are associated with temporal discounting in older adults. Neuropsychologia. 146, 107549. doi:10.1016/j.neuropsychologia.2020.107549.

Li, S., Wang, S., Li, X., Li, Q., Li, X., 2015. Abnormal surface morphology of the central sulcus in children with attention-deficit/hyperactivity disorder. Front. Neuroanat 9, 114. doi:10.3389/fnana.2015.00114.

Li, X., Hu, P., Liu, J., 2019. The neuroanatomical correlates of individual differences in delay discounting: a voxel-based morphometry study. J. Pacific Rim Psychol. 13.

Liu, Y., et al., 2014. Cortical thinning correlates with cognitive change in multiple sclerosis but not in neuromyelitis optica. Eur Radiol. 24 (9), 2334–2343. doi:10.1007/s00330-014-3239-1.

Liu, T., Wen, W., Zhu, W., Kochan, A.N., Trollor, N.J., Reppermund, S., Jin, S.J., Luo, S., Brodaty, H., Sachdev, S.P., 2011. The relationship between cortical sulcal variability and cognitive performance in the elderly. Neuroimage. 56 (3), 865–873. doi:10.1016/j.neuroimage.2011.03.015.

MacKillop, J., Amlung, M.T., Few, L.R., Ray, L.A., Sweet, L.H., Munafò, M.R., 2011. Delayed reward discounting and addictive behavior: a meta-analysis. Psychopharmacology 216 (3), 305–321. doi:10.1007/s00213-011-2229-0.

MacKillop, J., Amlung, M.T., Wier, L.M., David, S.P., Ray, L.A., Bickel, W.K., Sweet, L.H., 2012. The neuroeconomics of nicotine dependence: a preliminary functional magnetic resonance imaging study of delay discounting of monetary and cigarette rewards in smokers. Psychiatry Res. 202 (1), 20–29. doi:10.1016/j.pscychresns.2011.10.003.

MacKillop, J., Miller, J.D., Fortune, E., Maples, J., Lance, C.E., Campbell, W.K., Goodie, A.S., 2014. Multidimensional examination of impulsivity in relation to disordered gambling. Exp Clin Psychopharmacol 22 (2), 176–185. doi:10.1037/a0035874.

Madan, C.R., 2019. Robust estimation of sulcal morphology. Brain Inform. 6 (1), 5. doi:10.1186/s40708-019-0098-1.

Madan, C.R., 2021. Age-related decrements in cortical gyrification: Evidence from an accelerated longitudinal dataset. Eur J Neurosci. 53 (5), 1661–1671. doi:10.1111/ejn.15039.

Madan, C.R., Kensinger, E.A., 2016. Cortical complexity as a measure of age-related brain atrophy. Neuroimage 134, 617–629. doi:10.1016/j.neuroimage.2016.04.029.

Madan, C., Kensinger, A.E., 2017. Test–retest reliability of brain morphology estimates. Brain Inform. 4 (2), 107–121. doi:10.1007/s40708-016-0060-4.

Madden, G.J., Begotka, A.M., Raiff, B.R., Kastern, L.L., 2003. Delay discounting of real and hypothetical rewards. Exp. Clin. Psychopharmacol. 11 (2), 139–145. doi:10.1037/1064-1297.11.2.139.

Mandelbrot, B., 1985. Self-Affine Fractals and Fractal Dimension. Phys Scr. 21, 257–260. doi:10.1088/0031-8949/32/4/001.

Manuel, A.L., Murray, N.W.G., Piguet, O., 2019. Transcranial direct current stimulation (tDCS) over vmPFC modulates interactions between reward and emotion in delay discounting. Sci Rep 9 (1). doi:10.1038/s41598-019-55157-z.

Marek, S., Tervo-Clemmens, B., Calabro, F.J., Montez, D.F., Kay, B.P., Hatoum, A.S., … Dosenbach, N., 2020. Towards reproducible brain-wide association studies. bioRxiv 11, 15–18. doi:10.1101/2020.08.21.257758, Retrieved from.

Mohammadi, B., Hammer, A., Miedl, S.F., Wiswede, D., Marco-Pallarés, J., Herrmann, M., Münte, T.F., 2016. Intertemporal choice behavior is constrained by brain structure in healthy participants and pathological gamblers. Brain Struct. Funct. 221 (6), 3157–3170. doi:10.1007/s00429-015-1093-9.

Mazur, E.J., 1987. An adjusting procedure for studying delayed reinforcement. In: The effect of delay and of intervening events on reinforcement value. Lawrence Erlbaum Associates, Inc., pp. 55–73.

McClure, S.M., Laibson, D.I., Loewenstein, G., Cohen, J.D., 2004. Separate neural systems value immediate and delayed monetary rewards. Science 306 (5695), 503–507. doi:10.1126/science.1100907.

Myerson, J., Green, L., Warusawitharana, M., 2001. Area under the curve as a measure of discounting. J Exp Anal Behav 76 (2), 235–243. doi:10.1901/jeab.2001.76-235.

Nakagawa, S, Schielzeth, H, 2012. A general and simple method for obtaining R^2 from generalized linear mixed-effects models. Methods Ecol Evol. 4 (2), 133–142. doi:10.1111/j.2041-210x.2012.00261.x.

Owens, M.M., Duda, B., Sweet, L.H., MacKillop, J., 2018. Distinct functional and structural neural underpinnings of working memory. Neuroimage 174, 463–471. doi:10.1016/j.neuroimage.2018.03.022.

Owens, M.M., Gray, J.C., Amlung, M.T., Oshri, A., Sweet, L.H., MacKillop, J., 2017. Neuroanatomical foundations of delayed reward discounting decision making. Neuroimage 161, 261–270. doi:10.1016/j.neuroimage.2017.08.045.

Peters, J., Buchel, C., 2009. Overlapping and Distinct Neural Systems Code for Subjective Value during Intertemporal and Risky Decision Making. J Neurosci. 29 (50), 15727–15734.

Reishofer, G., Studencnik, F., Koschutnig, K., Deutschmann, H., Ahammer, H., Wood, G., 2018. Age is reflected in the Fractal Dimensionality of MRI Diffusion Based Tractography. Sci Rep. 8 (1), 5431. doi:10.1038/s41598-018-23769-6.

Rosch, K.S., Mostofsky, S.H., 2015. Increased delay discounting on a novel real-time task among girls, but not boys, with ADHD. J. Int. Neuropsychol. Soc. 22 (1), 12–23. doi:10.1017/S1355617715001071.

Schaer, M., Cuadra, B.M., Tamarit, L., Lazeyras, F., Eliez, S., Thiran, P.J., 2008. A surface-based approach to quantify local cortical gyrification. IEEE Trans Med Imaging 27 (2), 161–170. doi:10.1109/TMI.2007.903576.

Shamosh, N.A., Gray, J.R., 2008. Delay Discounting and Intelligence: a Meta-Analysis. Intelligence 36, 289–305.

Urošević, S., Youngstrom, E.A., Collins, P., Jensen, J.B., Luciana, M., 2016. Associations of age with reward delay discounting and response inhibition in adolescents with bipolar disorders. J. Affect. Disord. 190, 649–656. doi:10.1016/j.jad.2015.11.005.

Van Essen, D.C., 1997. A tension-based theory of morphogenesis and compact wiring in the central nervous system. Nature 385, 313–318.

Van Essen, D.C., Smith, S.M., Barch, D.M., Behrens, T.E., Yacoub, E., Ugurbil, K., 2013. The WU-Minn human connectome project: an overview. Neuroimage 80, 62–79. doi:10.1016/j.neuroimage.2013.05.041.

Van Essen, D.C., Ugurbil, K., Auerbach, E., Barch, D., Behrens, T.E., Bucholz, R., Chang, A., Chen, L., Corbetta, M., Curtiss, S.W., Della Penna, S., Feinberg, D., Glasser, M.F., Harel, N., Heath, A.C., Larson-Prior, L., Marcus, D., Michalareas, G., Moeller, S., Oostenveld, R., … Yacoub, E., 2012. The human connectome project: a data acquisition perspective. Neuroimage 62 (4), 2222–2231. doi:10.1016/j.neuroimage.2012.02.018.

Wallis, J.D., 2007. Orbitofrontal cortex and its contribution to decision-making. Ann. Rev. Neurosci. 30, 31–56. doi:10.1146/annurev.neuro.30.051606.094334.

Wang, Q., Chen, C., Cai, Y., Li, S., Zhao, X., Zheng, L., … Xue, G., 2016. Dissociated neural substrates underlying impulsive choice and impulsive action. Neuroimage 134, 540–549. doi:10.1016/j.neuroimage.2016.04.010.

Wilson, V.B., Mitchell, S.H., Musser, E.D., Schmitt, C.F., Nigg, J.T., 2011. Delay discounting of reward in ADHD: application in young children. J. Psychol. Psychia Allied Discip. 52 (3), 256–264. doi:10.1111/j.1469-7610.2010.02347.x.

Winkler, A.M., Ridgway, G.R., Webster, M.A., Smith, S.M., Nichols, T.E., 2014. Permutation inference for the general linear model. Neuroimage 92, 381–397.

Yang, F, Li, X, Hu, P, 2022. The Resting-State Neural Network of Delay Discounting. Front Psychol. 13, 828929. doi:10.3389/fpsyg.2022.828929.

Yu, R, 2012. Regional white matter volumes correlate with delay discounting. PloS one 7 (2). doi:10.1371/journal.pone.0032595.

Yun, H.J., Perez, J., Sosa, P., Valdés, J.A., Madan, N., Kitano, R., Akiyama, S., Skotko, B.G., Feldman, H.A., Bianchi, D.W., Grant, P.E., Tarui, T., Im, K., 2021. Regional alterations in cortical sulcal depth in living fetuses with down syndrome. Cereb Cortex (New York, N.Y. : 1991) 31 (2), 757–767. doi:10.1093/cercor/bhaa255.

Further reading

Im, K., Lee, J., Yoon, U., Shin, Y., Hong, B.S., Kim, Y.I., Kwon, S.J., Kim, K.I., 2006. Fractal dimension in human cortical surface: Multiple regression analysis with cortical thickness, sulcal depth, and folding area. Hum Brain Mapp 27 (12), 994–1003. doi:10.1002/hbm.20238.